④

Office of Naval Research

Contract N00014-87-K-0738

Task No. 431a020

Technical Report No. 1

PREPARATION AND MECHANISM OF FORMATION

OF SPHERICAL SUBMICRON ZnS POWDERS

by

Ahmet Celikkaya and Mufit Akinc

Prepared for Publication

in the

Journal of Colloid and Interface Science

Iowa State University

Department of Materials Science and Engineering

Ames, Iowa 50011

DTIC
SELECTED
JUL 0 8 1988
H

June 24, 1988

Production in whole or in part is permitted for any purpose of the
United States of Government

REPORT DOCUMENTATION PAGE

1a. REPORT SECURITY CLASSIFICATION	1b. RESTRICTIVE MARKINGS
Unclassified	

2a. SECURITY CLASSIFICATION AUTHORITY	3. DISTRIBUTION/AVAILABILITY OF REPORT
	Approved for public release
2b. DECLASSIFICATION/DOWNGRADING SCHEDULE	Distribution unlimited

4. PERFORMING ORGANIZATION REPORT NUMBER(S)	5. MONITORING ORGANIZATION REPORT NUMBER(S)
#1	N00014-87-K-0738

6a. NAME OF PERFORMING ORGANIZATION	6b. OFFICE SYMBOL (If applicable)	7a. NAME OF MONITORING ORGANIZATION
Iowa State University Mufit Akinc		Office of Naval Research Dr. R. Schwartz

6c. ADDRESS (City, State, and ZIP Code)	7b. ADDRESS (City, State, and ZIP Code)
	Code 38504 Naval Weapons Center China Lake, CA 93555-6001

8a. NAME OF FUNDING/SPONSORING ORGANIZATION	8b. OFFICE SYMBOL (If applicable)	9. PROCUREMENT INSTRUMENT IDENTIFICATION NUMBER

8c. ADDRESS (City, State, and ZIP Code)	10. SOURCE OF FUNDING NUMBERS

PROGRAM ELEMENT NO.	PROJECT NO.	TASK NO.	WORK UNIT NO.
			4312020

11. TITLE (Include Security Classification)

Preparation and Mechanism of Formation of Spherical Submicron ZnS Powders

12. PERSONAL AUTHOR(S)

Ahmet Celikkaya and Mufit Akinc

13a. TYPE OF REPORT	13b. TIME COVERED	14. DATE OF REPORT (Year, Month, Day)	15. PAGE COUNT
Technical	FROM _____ TO _____	88/06/24	25

16. SUPPLEMENTARY NOTATION

Submitted to Journal of Colloid and Interface Science

17. COSATI CODES			18. SUBJECT TERMS (Continue on reverse if necessary and identify by block number)
FIELD	GROUP	SUB-GROUP	

19. ABSTRACT (Continue on reverse if necessary and identify by block number)

20. DISTRIBUTION/AVAILABILITY OF ABSTRACT	21. ABSTRACT SECURITY CLASSIFICATION
☐ UNCLASSIFIED/UNLIMITED ☐ SAME AS RPT ☐ DTIC USERS	

22a. NAME OF RESPONSIBLE INDIVIDUAL	22b. TELEPHONE (Include Area Code)	22c. OFFICE SYMBOL

DD FORM 1473, 84 MAR

83 APR edition may be used until exhausted
All other editions are obsolete

SECURITY CLASSIFICATION OF THIS PAGE

PREPARATION AND MECHANISM OF FORMATION

OF SPHERICAL SUBMICRON ZnS POWDERS

Ahmet Celikkaya

and

Mufit Akinc

Department of Materials Science and Engineering

Iowa State University, Ames, IA   50011

July, 1988

ABSTRACT

Spherical, submicron particles of zinc sulfide were homogeneously precipitated by thermal decomposition of thioacetamide in acidic aqueous solutions. Rate of sulfide ion generation, determined by various combinations of temperature, pH, and initial concentrations of zinc ions and of thioacetamide, as related to particle growth rate had the paramount effect on the particle size distribution. Monosized, bimodal or narrow size distribution powders were obtained under certain combinations of experimental variables. Particles were found to be porous agglomerates of ~10 nm sphalerite crystallites. Particle growth was determined to proceed through diffusion-controlled aggregation of crystallites.

INTRODUCTION

Zinc sulfide is an attractive infrared window material as it possesses good IR transmittance in the 8-12 μm range as well as high melting temperature. When a polycrystalline material is used for applications such as this, a uniform final microstructure is needed. Although starting powders consisting of spherical, submicron particles are normally considered desirable, there is no general agreement as to whether particle assemblies with a narrow or a wide size distribution are more preferable for achieving a theoretically dense uniform microstructure. It is well known that random packing of particles with a size distribution yields denser green compacts than do monosize particles. On the other hand, monosize powder assemblies are believed to sinter more uniformly and so result in a more uniform sintered microstructure. Ability to control precipitation variables in order to yield reproducible ceramic powders with spherical, submicron particles having a specific type of particle size distribution in sufficient quantities is a prerequisite to the understanding of variables that influence packing efficiency and uniformity of initial and final microstructure.

Zinc sulfide has long been prepared by a variety of methods, including gas phase, solid/vapor and aqueous solution reactions (1-5). Chiu (3) was the first to prepare monosized, spherical particles of sulfides of several metals including zinc. His procedure involved complexing zinc ions with EDTA followed by precipitation by bubbling H_2S gas through the solution. A mean particle diameter of 0.2 μm was obtained employing very low zinc

1

ion concentrations ($<10^{-3}$M). Later, Wilhelmy and Matijevic (4) employed thermal decomposition of thioacetamide (TAA) to prepare micron-sized spherical particles by aging the reaction mixture several hours using a two step procedure. Williams et al. (5) employed the same technique to prepare monosized, spherical particles of ZnS about 3 µm in diameter. In this case, however, the critical nuclei appeared as faceted single crystals rather than the spherical, submicron "seeds" observed by Wilhelmy and Matijevic, and the resulting powder was a mixture of sphalerite (cubic) and wurtzite (hexagonal) phases.

The main objective of this work was to investigate the influence of experimental variables on the morphology of the ZnS particles produced by thioacetamide decomposition and to understand the mechanism of particle formation.

EXPERIMENTAL

A. Materials: Reagent grade TAA (99% pure) was supplied by Aldrich Chemical Co. All other chemicals, used in this study were Fisher Reagent grade and were used without further purification.
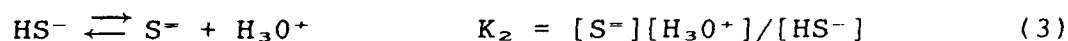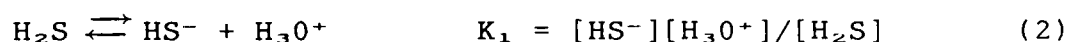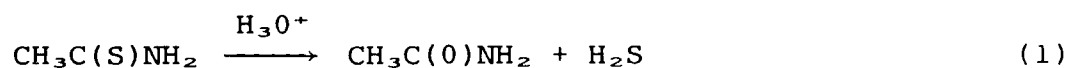
B. Precipitation: A stock solution of zinc ions was prepared by dissolving $Zn(NO_3)_2 \cdot 6H_2O$ in deionized water and then filtering through 0.1 μm cellulose nitrate membrane filters to give a final zinc ion concentration of 1.56 M. An 8.3 mL aliquot of this stock was transferred into a beaker and nitric acid solution (0.1 N or 0.01 N) was added to bring the total volume slightly less than 250 mL. The solution was heated to reaction temperature, the desired amount of thioacetamide was added and final volume was brought to 250 mL. The beaker was then immersed in a water bath at the set reaction temperature. After a certain period of aging, a bluish tint in the solution was judged to indicate the onset of precipitation. The time interval necessary to induce the change in the solution color was recorded. Thirty milliliter aliquots were collected and quenched to 15°C periodically after precipitation had started. A number of combinations of experimental variables were investigated: Aging temperature of 60, 70, and 80°C were employed. Initial thioacetamide concentrations were varied to give $[TAA]_o/[Zn]_o$ ratios of 4, 8 and 16 for pH = 1 and pH = 2. Initial zinc ion concentration $[Zn]_o$ was held constant at 0.05 M in all experiments.

C. Characterization: The change of particle size distribution over time was determined by a centifugal particle size analyzer using a portion of 30 mL aliquots collected at various times during the aging process. The remainder of the aliquot was centrifuged at 5000 rpm for 30 min. and the recovered precipitate was washed once with deionized water and once with acetone. A drop of suspension in acetone was placed on an aluminum foil and dried for observation of morphology by SEM. Selected area electron diffraction patterns were obtained to determine structure of individual particles. X-ray diffraction spectra of the powders were also obtained to determine crystallite sizes and phase purity of the powders. Specific surface areas of the powders were determined by a single point BET method using a N_2-He gas mixture.

RESULTS AND DISCUSSION

A. Determination of critical supersaturation:

Homogeneous precipitation of zinc sulfide by thermal decomposition of thioacetamide in acidic (pH < 3) aqueous solutions proceeds as follows:

$$CH_3C(S)NH_2 \xrightarrow{\quad H_3O^+ \quad} CH_3C(0)NH_2 + H_2S \tag{1}$$

$$H_2S \rightleftharpoons HS^- + H_3O^+ \qquad K_1 = [HS^-][H_3O^+]/[H_2S] \tag{2}$$

$$HS^- \rightleftharpoons S^= + H_3O^+ \qquad K_2 = [S^=][H_3O^+]/[HS^-] \tag{3}$$

Swift and Butler (6) had studied the kinetics of TAA decomposition, the rate determining step, and found a rate expression of

$$- \frac{d[TAA]}{dt} = k[H_3O^+][TAA] \tag{4}$$

For the rate constant, k, an Arrhenius type expression was found with a pre-exponential factor of 6.58×10^{11} L.mole^{-1}.min^{-1} and an activation energy of 79.87 kJ.mole^{-1}. The total concentration of sulfide species at time t can then be found by recognizing that $[TAA]_o - [TAA]_t = [S]_{total} = [H_2S] + [HS^-] + [S^=]$ and integrating equation (4) from t = 0 to t = t to give:

$$[TAA]_o (1 - exp(-k[H_3O^+]t)) = [H_2S] + [HS^-] + [S^=] \tag{5}$$

Combining equation (5) with (2) and (3) yields:

5

$$[TAA]_o \, (1-\exp(-k[H_3O^+]t)) = \frac{[H_3O^+]^2[S^-]}{K_1K_2} + \frac{[H_3O^+][S^-]}{K_2} + [S^-] \quad (6)$$

or, equivalently stated

$$[S^-] = \frac{[TAA]_o \, (1-\exp(-k[H_3O^+]t))}{[H_3O^+]^2/K_1K_2 + [H_3O^+]/K_2 + 1} \quad (7)$$

Accurate thermodynamic data are available in the literature for the dissociation reactions of H_2S and the formation of aqueous sulfide species at room temperature (7). Assuming that ΔH° and ΔS° are constant over the temperature range studied, values of K_1, K_2 and solubility product K_{sp} for zinc sulfide at any temperature can easily be calculated. Expressions for these constants were calculated to be:

$$K_{1,T} = 8.71 \times 10^{-4} \exp \, (-5404.80/RT) \quad (8)$$

$$K_{2,T} \; 5919.46 \exp \, (-24195.56/RT) \quad (9)$$

$$K_{sp,T} = 2.30 \times 10^{-10} \exp \, (-17575.45/RT) \quad (10)$$

where R is the gas constant in Joules per mole per degree Kelvin. Using this information, the relative supersaturation at any time t, which is defined as

6

$$S = \left[\frac{[Zn^{2+}]_t [S^-]_t}{K_{sp}} \right]^{\frac{1}{2}} \qquad (11)$$

can be calculated for any combination of T, pH and initial

concentrations of TAA and zinc ions. Figure 1 shows the variation

of S with time for various combinations of experimental parameters,

assuming that no precipitation occurs. Also indicated on these

curves are the times at which precipitation started with

corresponding values of critical supersaturation for that

particular combination of experimental variables. The value of

critical supersaturation for nucleation remained more or less

constant around 8.5 in each case. This value of critical

supersaturation found is an order of magnitude less than what

Williams et al. (5) report. The difference arises mainly due to

differences in the K_{sp} values used. Williams et al. used a K_{sp} of

4.8×10^{-23} at 75°C whereas we estimated a value of 2.13×10^{-21} at the

same temperature for cubic ZnS. All other constants used were of

the same magnitude. Another contribution to the observed

difference may arise from a stronger interaction between Zn^{++} and

the SO_4^- ions in the solution which they have employed as a

supporting anion as opposed to the NO_3^- in our study. Our

experiments using sulfate salts showed a strong effect of SO_4^-

ions on the precipitation kinetics (8).

B. Effect of sulfide ion generation rate on particle size

distribution:

   Although the absolute value of relative supersaturation at the

time of nucleation remained constant for various combinations of

7

experimental parameters, the time needed to reach the critical relative supersaturation varied over two orders of magnitude. The reciprocal time to reach critical supersaturation is related to sulfide ion generation rate in the solution, and we have defined it as the 'rate-to-nucleation' for the context of this study. Table 1 gives the rate-to-nucleation for several combinations of experimental variables at $[Zn]_o = 0.05$ M. Rate-to-nucleation had the paramount influence on the particle size distribution of the powders. Rates higher than 0.250 min^{-1} was the range where most variability in particle size distribution was observed

Figure 2 shows an electron micrograph taken 180 min. after precipitation had started for run #2 (pH = 1, T = 60°C, $[Zn]_o$ = 0.05 M and $[TAA]_o/[Zn]_o$ = 8) corresponding to a rate of 1.41×10^{-2} min^{-1}. Formation of the particles was first observed after 70 min. Growth of these particles with time is given in curve 'a' of Figure 3. The drop in the mean particle size for this run at 180 minutes is a result of formation of a second generation of particles, as may be observed in the electron micrograph of Figure 2. Similar bimodal size distributions were observed for rate-to-nucleation values of up to 0.250 min^{-1}, with higher growth rates, as indicated by higher slopes of curves b and c in Figure 3, and shorter times for formation of second generation of particles, as demonstrated by the shift of maxima toward shorter times.

At least two plausible explanations can be offered for observing two generations of particles. First, as the initially formed particles reach a critical size (typically $\geq 1\mu m$) where they can settle out of the solution, a new generation of particles

8

Table I - Variation of rate of sulfide ion generation with various combinations of experimental parameters.

Run #	Temperature (°C)	pH	$[TAA]_o/[Zn]_o$	Rate to Nucleation (min^{-1})
1	60	1	4	6.6×10^{-3}
2	60	1	8	1.41×10^{-2}
3	70	1	4	2.70×10^{-2}
4	70	1	8	5.88×10^{-2}
5	70	1	16	1.11×10^{-2}
6	70	2	4	0.250
7	70	2	8	0.500
8	70	2	16	1.00
9	80	2	4	1.50
10	80	2	8	2.00
11	80	2	16	4.00

may form from the solution. Secondly, if the rate of sulfide ion formation is slightly larger than the rate of its consumption in the growth process, a build up of excess sulfide ions may result in formation of a second generation of particles. The first mechanism does not appear to be likely as calculations based on the limiting size of first generation particles show that settling times are approximately the same as the total aging time.

At intermediate rates, such as 0.250 to 1.00 min^{-1}, the population density of first generation particles is high enough that growth of these particles can maintain [S^-] low enough to prevent formation of second generation particles and hence monosize particles are obtained. Figure 4 shows micrographs of precipitates for run #7 at various precipitation times. The precipitation was completed (~100% recovery), in approximately one hour with a final mean particle size of about 0.5 μm.

At still higher rates-to-nucleation (specifically at around 1.00 to 1.50 min^{-1}), a bimodal particle size distribution was as in obtained, with larger particles (first generation) having a mean size of about 0.6 μm at the end of precipitation. A scanning electron micrograph of such a sample is given in Figure 5. Observation of bimodal size distribution at high rates supports the earlier paradigm that second generation of particles is a direct consequence of growth rate not keeping up with the sulfide ion generation rate, resulting in a net sulfide ion build-up in the solution.

Beyond a rate of 1.50 min^{-1}, a continuous distribution of particle sizes was obtained as shown by the electron micrograph of

10

particles obtained for run #10 in Figure 6. As indicated in the figure, particle size ranges between 0.2 and 0.5 μm and distribution is continuous.

C. Mechanism of Particle Formation and Growth:

Specific surface area values for a larger number of samples were found to be around 50 m²/g. This value of surface area is much higher than the value of 4.87 m²/g expected for a monosize powder having a mean particle diameter of 0.3 μm, and corresponds to an equivalent spherical diameter of about 29 nm. The apparent discrepancy between the observed mean particle diameter and the equivalent spherical diameter, calculated from specific surface area value, can be resolved if one assumes that the large particles (~0.3 μm) are extremely porous or are collections of much smaller (~29 nm) crystallites.

A transmission electron micrograph and selected area diffraction pattern of a monosize powder are shown in Figure 7. As the figure clearly indicates, the spherical particles are actually agglomerates of about 14 nm crystallites which the diffraction pattern shows to be sphalerite. An independent determination of the crystallite size was made with the x-ray diffraction line broadening technique. The crystallite size was found to be 13 nm, in reasonably good agreement with the values obtained by surface area and TEM observations.

Alternatively, one can estimate the size of the nuclei that form during the precipitation using a modified form of the Kelvin equation (9):

11

$$\frac{RT}{M} \ln \frac{a_r^*}{a} = \frac{2\gamma}{\rho r^*} \tag{12}$$

where a_r^* is the activity of the ions in equilibrium with a nucleus having a critical radius r^*, a is the activity of ions in equilibrium with a macroscopic crystal phase, γ is the interfacial tension between solid and liquid phase, ρ is the density of the solid, M is the molecular weight, R is the gas constant and T is the absolute temperature. Comparison of this equation with equation (11), and assuming that the activity coefficient is unity and that the ionic strengths of the solution in equilibrium and in supersaturated condition are roughly the same (10), gives

$$2 \frac{RT}{M} \ln S = \frac{2\gamma}{\rho r^*} \tag{13}$$

Using this equation and substituting 1.672 J/m² for (for the {100} face of sphalerite) and a density of 4.10 Mg/m³, the critical nucleus size at a relative supersaturation of 8.5 is found to be 13 nm, which is in excellent agreement with the crystallite sizes determined experimentally. This implies that the nuclei, once formed, do not grow significantly and growth of spherical particles occurs through agglomeration of 13 nm size sphalerite crystallites. The agglomeration time necessary to reduce the population of these crystallites by half is estimated to be less than one second assuming no barrier for agglomeration. Since the precipitation was carried at low pH near its isoelectric point (4), agglomeration is likely to proceed quite rapidly preventing growth of individual nuclei.

12

A straight line was obtained when the diffusion chronomal, I_D, was plotted against time for particle growth of monosized powders for run #7 (Figure 7) indicating that the growth was a diffusion controlled process (11). Diffusion coefficient, D, is proportional to the slope of I_D versus t plot and estimated to be about 10^{-6} cm^2/sec, which is about an order of magnitude less than that of ionic species in aqueous solutions. Such a low diffusion coefficient confirms that the growth of the spherical particles proceeds by diffusion of crystallites through the depleted aqueous layer. Similar observations were reported by Bleier and Cannon (12) for formation of uniform m-ZrO$_2$ particles and by Edelson and Gleaser (13) for spherical TiO$_2$ particles.

Formation of monosize particles at moderate rates may be explained in light of the above agglomeration mechanism. If the rate of crystallite generation is comparable to that of diffusion of these crystallites to deposit on the growing agglomerate, then the agglomerates will grow uniformly to produce monosized particles. If on the other hand, the crystallite generation rate is higher than the diffusion rate, then the population of these crystallites may reach a critical value at which second generation of particles forms, resulting in a bimodal size distribution. Figure 8 shows schematically the formation mechanism for bimodal size distribution. Figure 8a represents the formation of crystallites in the solution. High concentration of crystallites result in agglomeration of nearly uniform size spherical particles as predicted by estimated agglomeration rate (Figure 8b). Broken circles around each agglomerate represents the aqueous layer with

13

depleted crystallite concentration. Since the sulfide ion
generation rate is considerably high, a large number of new
crystallites form throughout the solution. Crystallite population
outside the layer builds up while those crystallites that form
within the layer contribute to the growth of agglomerates (Figure
8c). As soon as the crystallite concentration outside the layer
reaches to a critical value, a second agglomeration event takes
place, resulting in a second generation of agglomerates which are
smaller than the first generation as shown in Figure 8d. A very
high percentage of crystallites forming afterwards is consumed in
the growth process due to the large number of growing agglomerates.
Depending on the sulfide ion generation rate, it is possible that
multiple agglomeration events may occur resulting in a wide
particle size distribution as is shown in Figure 6.

CONCLUSION

Formation of uniform spherical particles of ZnS was investigated, with primary consideration being given to the influence of experimental variables on the morphology. It was determined that nucleation starts at a constant supersaturation level of 8.5 for a number of combinations of experimental variables. Type of particle size distribution was found to be controlled by the rate at which this critical nucleation event is reached (i.e. the rate-to-nucleation), irrespective of the value of the individual variables. Furthermore, rate-to-nucleation was determined to be significant that the nucleation is primarily controlled by the rate of sulfide ion generation at constant zinc concentration.

The mechanism of particle formation is believed to follow a two-step process with the formation of nuclei of about 10 nm size then aggregation of these crystallites to form spherical particles consisting of clusters of about 0.3 to 1.0 μm size. The type of the particle size distribution was controlled by two competing processes, rate of sulfide ion generation and rate of growth of agglomerates. Spherical submicron ZnS powders with desired size distribution were produced reproducibly by controlling the rate of sulfide ion generation.

15

ACKNOWLEDGEMENTS

16

REFERENCES

1. Miles, P. A., J. Opt. Soc. Am. 63, 1323 (1973)

2. Leverenz, H. W., Science 109, 183 (1929).

3. Chiu, G., J. Coll. and Int. Sci. 83(1), 309 (1981).

4. Wilhelmy, D. M. and Matijevic, E., J. Chem. Soc., Faraday Trans. 1 80, 563 (1984).

5. Williams, R., Yocom, P. N. and Stofko, F. S., J. Coll. and Int. Sci. 106(2), 388 (1985)

6. Swift, E. H., Butler, E. A., Anal. Chem., 28(2), 146, (1956).

7. Harris, D. C., "Quantitative Chemical Analysis, 2nd Edition", pp. 725, 726. W. H. Freeman and Company, New York, 1987.

8. Celikkaya, A. and Akinc, M., unpublished work.

9. LaMer, V. K. and Dinegar, R. J., Am. Chem. Soc. 73, 3280 (1951).

10. Akinc, M., Proposal Submitted to Office of Naval Research 1986.

11. Nielsen, A. E., "Kinetics of Precipitation", pp. 29-39. The Macmillan Company, New York, 1964.

12. Bleier, A., and Cannon, R. M., in "Better Ceramics Through Chemistry II", (Brinker, C. J., Clark, D. E., Ulrich, D. R., Eds.), p. 71. Materials Research Society, Pittsburgh, Pennsylvania, 1986.

13. Edelson, L. H., and Gleaser, A. M., J. Am. Ceram. Soc. 71(4), 225 (1988).

FIGURE CAPTIONS

Figure 1.   Variation of relative supersaturation S with time for
             various combinations of experimental parameters with
             $[Zn]_o$ = 0.05 M and
             a) pH = 1, T = 60°C, $[TAA]_o]/[Zn]_o$ = 4
             b) pH = 1, T = 60°C, $[TAA]_o]/[Zn]_o$ = 8
             c) pH = 1, T = 70°C, $[TAA]_o]/[Zn]_o$ = 4
             d) pH = 2, T = 60°C, $[TAA]_o]/[Zn]_o$ = 4
             Values of critical supersaturation are also indicated
             for each case.

Figure 2.   Scanning Electron micrograph of particles obtained (with
             experimental parameters pH = 1, T = 60°C, $[Zn]_o$ = 0.05 M
             and $[TAA]_o/[Zn]_o$ = 8) 180 min. after precipitation
             started.

Figure 3.   Variation of mean particle size with time for pH = 1,
             $[Zn]_o$ = 0.05 M and a) $[TAA]_o/[Zn]$ = 8, T = 60°C.
             b) $[TAA]_o/[Zn]$ = 4, T = 70°C   c) $[TAA]_o/[Zn]_o$ = 8,
             T = 70°C.

Figure 4.   Scanning electron micrographs of particles obtained with
             experimental parameters being pH = 2, T = 70°C, $[Zn]_o$
             0.05 M and $[TAA]_o/[Zn]_o$ = 8.   a) 5, b) 10, c) 15, d) 40
             mins. after precipitation started.

Figure 5.   Scanning electron micrograph of ZnS particles obtained
             under the conditions pH = 2, T = 80°C, $[Zn]_o$ = 0.05 M
             and $[TAA]_o/[Zn]_o$ = 4.

Figure 6.   Scanning electron micrographs of ZnS particles obtained
             when pH = 2, T = 80°C, $[Zn]_o$ = 0.05 and
             a) $[TAA]_o/[Zn]_o$ = 8, b) $[TAA]_o/[Zn]_o$ = 16.

Figure 7.   Transmission electron micrograph of sample given in
             Figure 4b and selected area diffraction pattern of the
             particles.

Figure 8.   Schematic diagram of mechanism of particle formation and
             growth for a case yielding a bimodal size distribution.
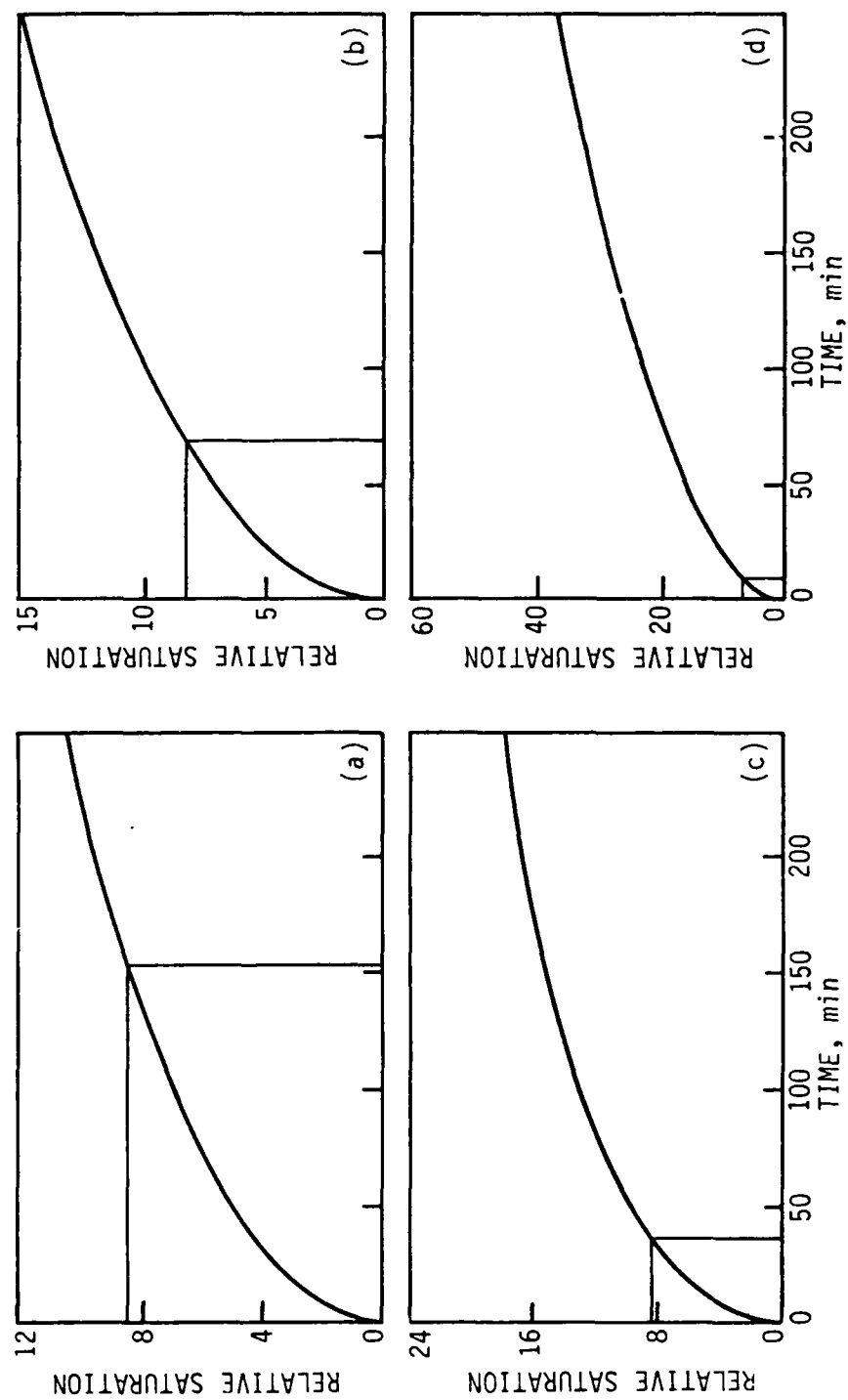
Figure 1   Celikkaya/Akinc
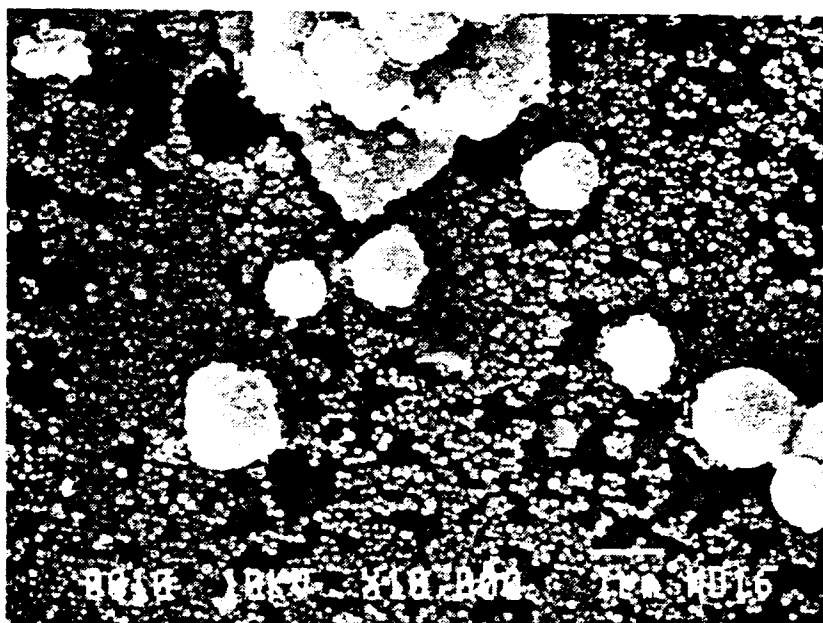
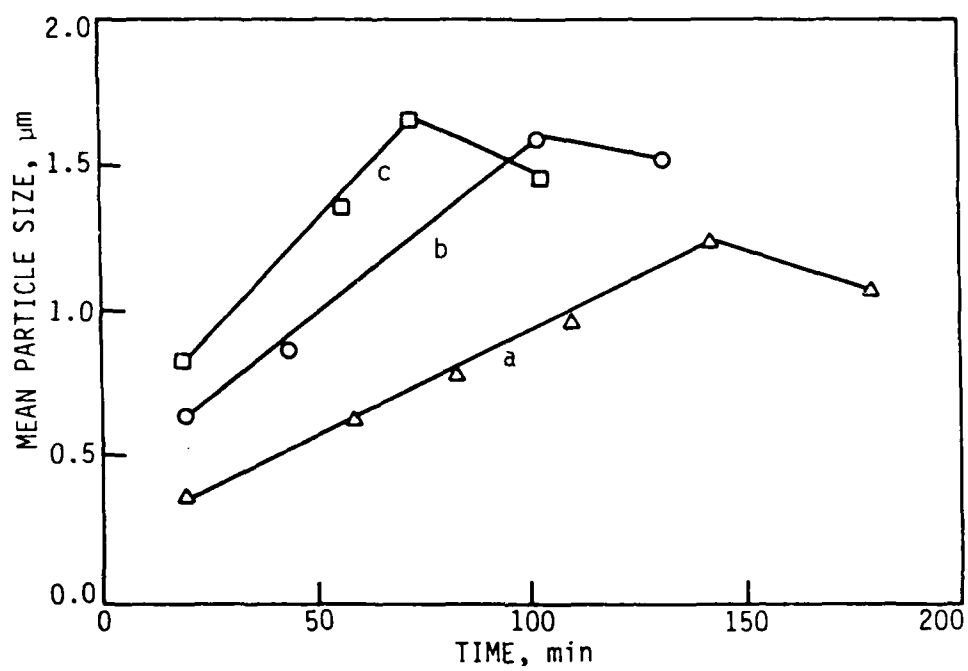Figure 2   Celikkaya/Akinc

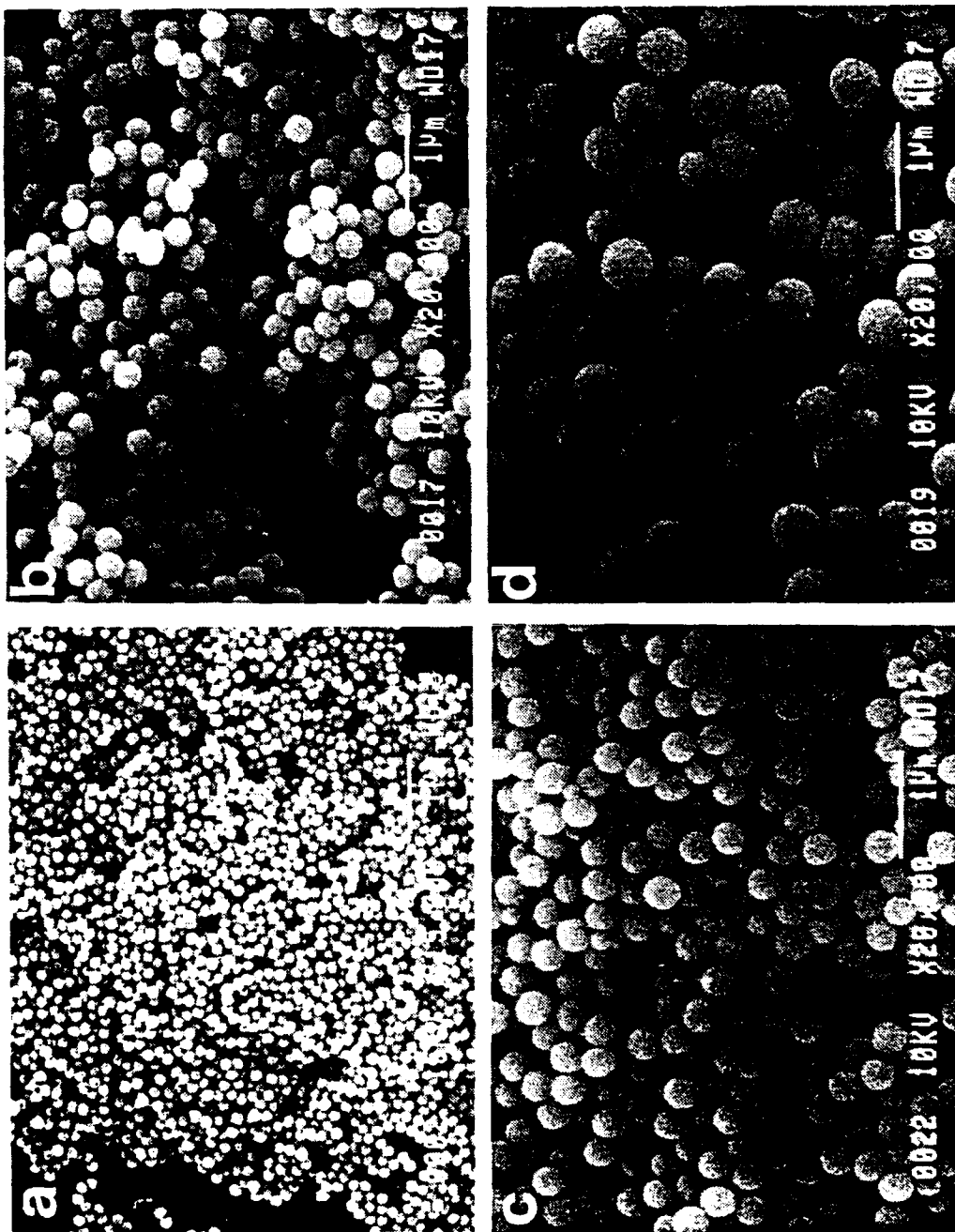Figure 3   Celikkaya/Akinc

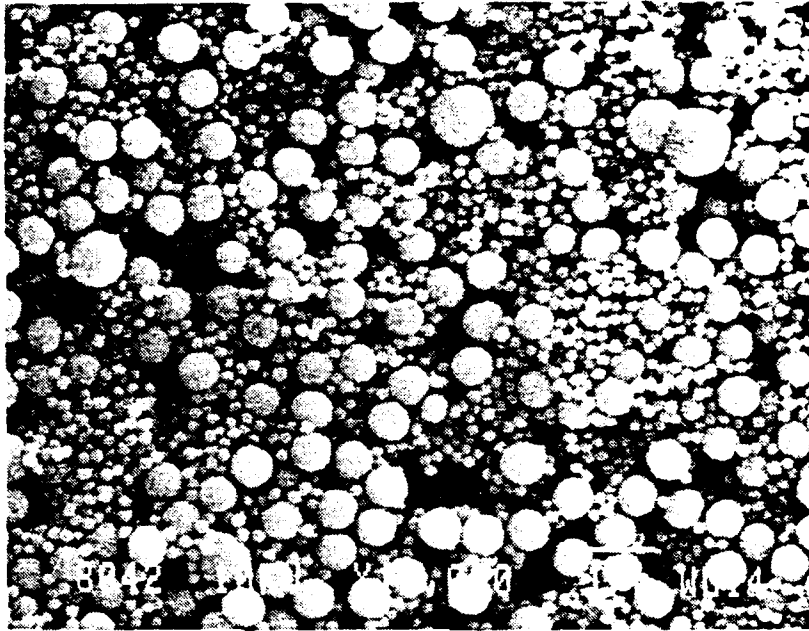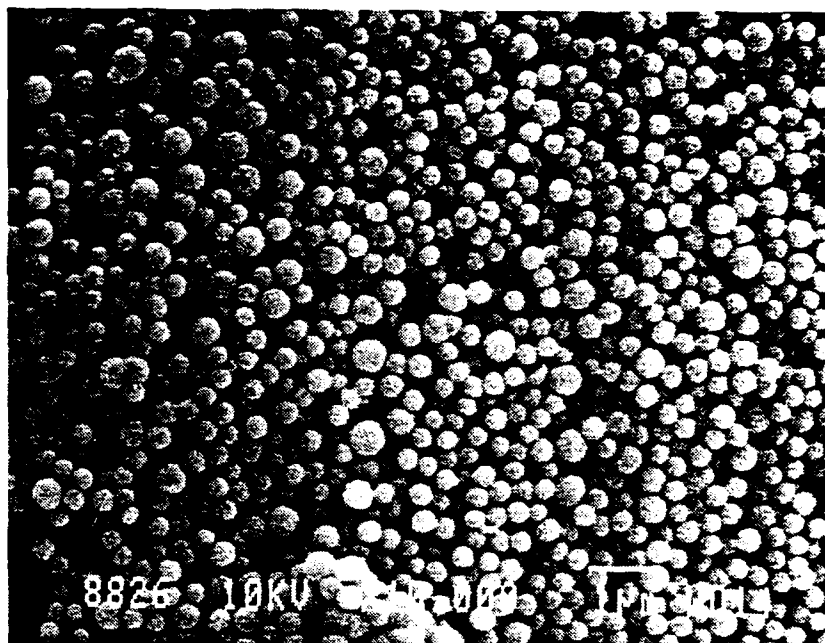Figure 4   Celikkaya/Akinc

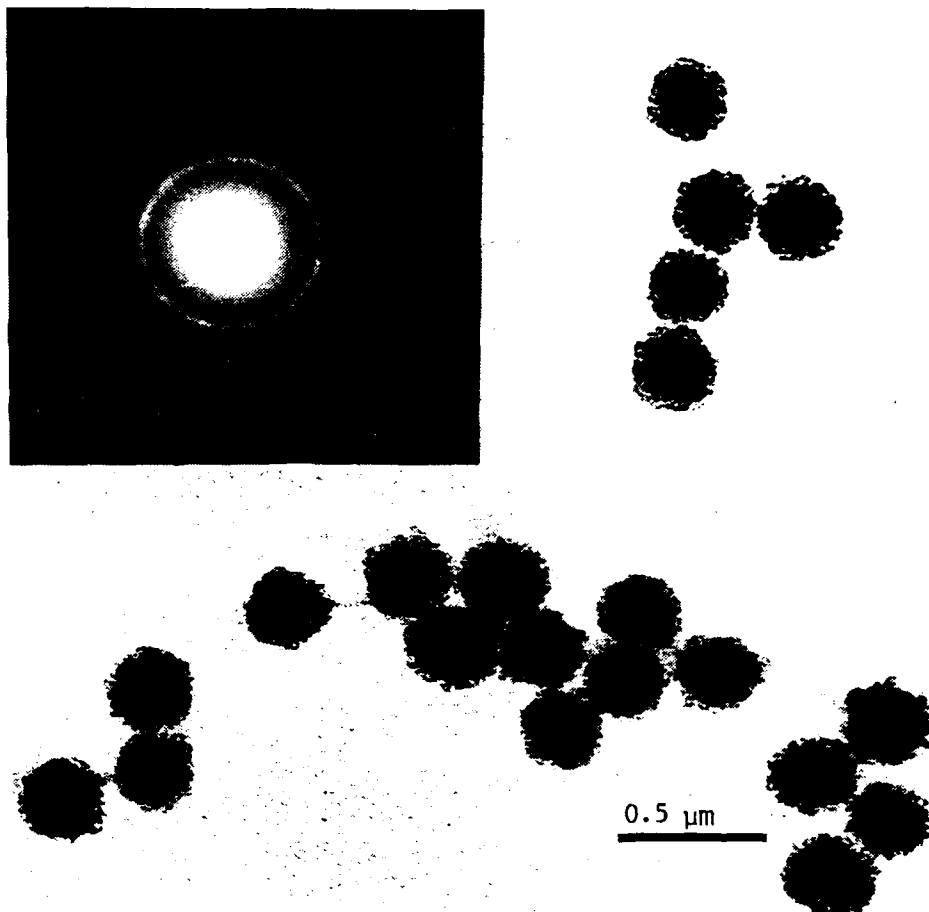Figure 5   Celikkaya/Akinc

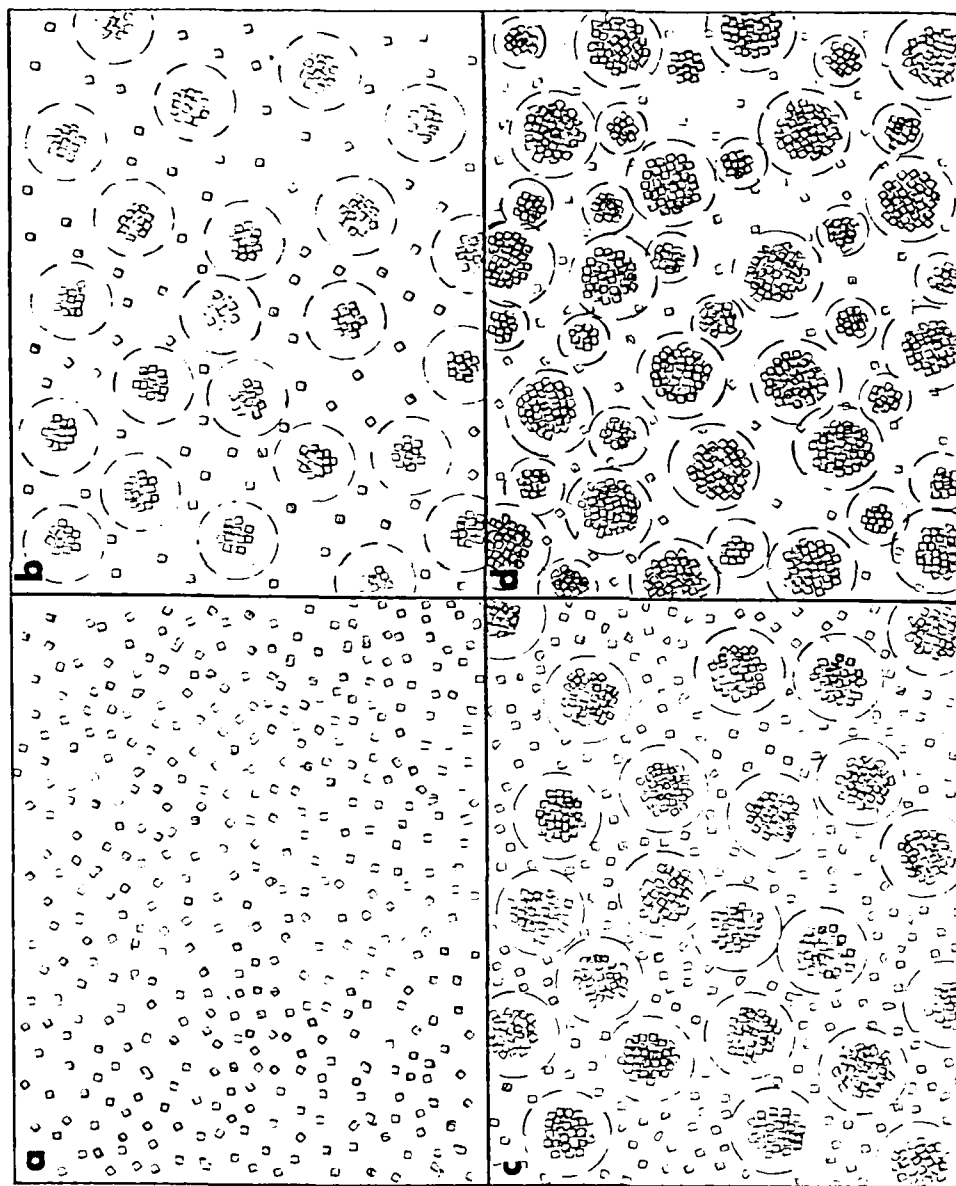Figure 6   Celikkaya/Akinc

Figure 7   Celikkaya/Akinc

Figure 8   Celikkaya/Akinc

Dr. Mufit Akinc
Mat'ls Science&Eng.Dept
Iowa State University
110 Engineering Annex
Ames, IA 50011

Dr. H. E. Bennett
Code 38101
Naval Weapons Center
China Lake, CA 93555

Dr. C. Blackmon
Code G23
Naval Surface WeaponsCtr
Dahlgren, VA 22448

Dr. S. Block
Group Leader
Structural Chemistry
National Bureau of
  Standards
Gaithersburg, MD 20899

Dr. J. Burdett
Chemistry Department
University of Chicago
Chicago, IL 60637

Dr. J. A. Cox
Honeywell Systems and
  Research
Dept. MN 65-2600
1660 Technology Drive
Minneapolis, MN 55418

Mr. B. Dunn
Materials Science and
  Engineering Department
Univ. of California, LA
Los Angeles, CA 90024

Dr. G. Geoffroy
Chemistry Department
Pennsylvania State Univ.
University Park,PA 16802

Dr. A. Harker
Rockwell International
P.O. Box 1085
Thousand Oaks, CA 91360

Dr. D. C. Harris
Code 3854
Naval Weapons Center
China Lake, CA 93555

Optical

Dr. R. A. Heinecke
StandardTelecommunication
  Laboratories, Ltd
London Road
Harlow, Essex CM17 9NA
England

Dr. T. A. Hewston
Code 3854
Naval Weapons Center
China Lake, CA 93555

Dr. M. E. Hills
Code 3854
Naval Weapons Center
China Lake, CA 93555

Dr. Lisa C. Klein
Ctr.forCeramics Research
College of Engineering
Rutgers University
P.O. Box 909
Piscataway, NJ 08854

Dr. P. Klocek
Texas Instruments
P. O. Box 660246
Dallas, TX 75266

Dr. D. N. Lewis
Code 6360
Naval Research Lab
Washington, DC 20375

Ms. D. J. Martin
AFWL/ARBE
Kirtland AFB, NM 87117

Dr. Y. Mehrotra
Perkin-Elmer Company
100 Wooster Heights Road
Danbury, CT 06810

Dr. P. Melling
Ceramics&Glass Technology
Battelle Columbus Labs
Columbus, OH 43201

Dr. R. Messier
Pennsylvania State Univ.
Materials Research Lab
University Park,PA 16802

Ceramics

Dr. G. Messing
Materials Research Dept.
Pennsylvania State Univ.
University Park,PA 16802

Dr. Harry Moreen
Rockwell International
3370 Mira Loma Avenue
Anaheim, CA 92803

Dr. P. E. D. Morgan
Rockwell Science Center
P.O. Box 1085
Thousand Oaks, CA 91360

Dr. S. Musikant
General Electric Co
P. O. Box 8555
Philadelphia, PA 19101

Mr. P. Ormsby
U.S. Army Missile Cmd.
Redstone Arsenal
Huntsville, AL 35807

Dr. C. Pantano
Materials Science Lab
Pennsylvania State Univ.
University Park,PA 16802

Dr. Dale Perry
U.S. Army Missile Cmd.
Redstone Arsenal
Huntsville, AL 35807

Dr. John C. Pulver
Department 144
Eastman Kodak Company
HawkeyePlantApparatusDiv
901 Elmgrove Road
Rochester, NY 14650

Dr. R. Raj
Materials Science and
  Engineering Department
Cornell University
Ithaca, NY 14853

Dr. W. Rhodes
GTE Laboratories
40 Sylvan Road
Waltham, MA 02134

Mr. R. Rice
W. R. Grace Company
7379 Route 32
Columbia, MD 21044

Mr. D. Roy
Coors Porcelain Company
Golden, CO 80401

Dr. R. Roy
Materials Science Lab
Pennsylvania State Univ.
University Park,PA 16802

Dr. J. Savage
Royal Signals and Radar
  Establishment
St. Andrews Road
Great Malvern,
WORCS, WRI4 3PS
England

Dr. R. W. Schwartz
Code 3854
Naval Weapons Center
China Lake, CA 93555

Dr. A. Stacy
Chemistry Department
Univ. of Calif.,Berkeley
Berkeley, CA 94720

Dr. I. G. Talmy,Code R31
Naval Surface WeaponsCtr
White Oak Laboratory
Silver Spring, MD 20903

Mr. W. Tropf
Applied Physics Lab
Johns Hopkins Road
Laurel, MD 20810

Dr. R. Tustison
Raytheon Co.Research Div
131 Spring Street
Lexington, MA 02173

Dr. W. White
Materials Research Lab
Pennsylvania State Univ.
University Park,PA 16802

Dr. A. Wold
Chemistry Department
Brown University
Providence, RI 02912